ELSEVIER

Earth and Planetary Science Letters 199 (2002) 211–226

EPSL

www.elsevier.com/locate/epsl

Dynamics of obsidian flows inferred from microstructures: insights from microlite preferred orientations

Jonathan Castro [a,*], Michael Manga [b], Katharine Cashman [c]

[a] *Department of Geology, 52 W. Lorain St. Oberlin College, Oberlin, OH 44074, USA*
[b] *Earth and Planetary Science, U.C. Berkeley, 307 McCone Hall, Berkeley, CA 94720-4767, USA*
[c] *1272 Geological Sciences, University of Oregon, Eugene, OR, 94703-1272, USA*

Received 5 December 2001; received in revised form 14 February 2002; accepted 21 February 2002

Abstract

The flow of obsidian lava leads to crystal alignments that reflect both the accumulated strain and the type of flow across the surface. Microlite preferred orientations are used to investigate the emplacement dynamics, strain history, and structural evolution of Obsidian Dome, eastern California. Measurements of three-dimensional microlite trend and plunge in samples from the near-vent region, distal flow, and flow front show: (1) the flow directions along the dome margins, (2) the deformation style (e.g., pure versus simple shear) at the dome margins, and (3) the variation in strain as a function of position within the flow. Microlites form well-developed lineations in the plane of flow banding in all samples. Stereographic projections indicate that lineations trend normal to the western flow front and plunge shallowly away from the margin. The radial flow pattern indicated by measurements made along the western margin suggests that extrusion was from a roughly elliptical vent. These results highlight a strong correlation between microlite trend and the bulk flow direction inferred from the geometry of the flow. Along most of the eastern periphery, lineations trend parallel to the margin and likely reflect the local flow direction as influenced by compression against the thickening flow crust, marginal talus piles, and topography. Orientation distributions imply that radial spreading accompanied by flattening was the dominant mechanism for flow emplacement. Comparisons of measured orientation distributions with theoretical predictions suggest that microlite fabrics in flow front and near-vent samples developed in a pure shear flow. Microstructures in a sample from near the distal flow base records a component of simple shear. Variance in microlite trend provides a measure of the amount of strain acquired during flow. Standard deviation in trend decreases from the near-vent region to the flow margins, reflecting progressive alignment of microlites during transport. Pure shear strain inferred from orientation distributions increases from approximately 0.3 near the vent to about 1.1 at the flow front. The difference between these strains (0.8) is an estimate of the strain associated with flow emplacement. Such strain is similar in size to that estimated from mesoscopic structures ($\sim$1) and for horizontal spreading of a fluid whose volume is equal to that of Obsidian Dome ($\sim$1.6). This suggests that flow on the surface was sufficient to produce observed microlite preferred orientations in the flow front. These techniques can be applied to interpret older dissected lavas where erosion has erased much of the original flow front or where larger-scale structures indicative of flow directions are poorly preserved.

* Corresponding author. Tel.: +1-440-775-6701; Fax: +1-440-775-8038. *E-mail address:* jcastro@oberlin.edu (J. Castro).

0012-821X/02/$ – see front matter
PII: S0012-821X(02)00559-9

Keywords: obsidian; microlite; emplacement; strain; kinematics

1. Introduction

Flow structures in solidified lavas record strain developed during motion and thus contain important kinematic information about flow emplacement processes. The emplacement history of a lava flow is defined by its displacement directions, flow type (i.e., strain regime), and finite strain. These characteristics vary both temporally and spatially, thus an accurate assessment of lava flow kinematics requires detailed structural analysis at several scales. For example, AMS studies [1] and analyses of crystal preferred orientation [2,3] can be used to determine paleoflow directions and paleoslopes. Crystal preferred orientations [2,3], folds [4–6] and deformed enclaves [7–9] have been used as rheologic and kinematic indicators to infer the fluid dynamics of silicic dome and flow emplacement. These techniques are particularly important for the analysis of flows that were not observed when active, and thus lack observational constraints on their emplacement dynamics and histories.

Silicic lavas (dacites and rhyolites) have been the focus of a range of kinematic and dynamic studies [5,9,10]. For example, the geometry of large-scale folds and flow banding patterns in rhyolite flows suggests that flow in the vent regions of silicic domes is dominated by coaxial spreading (i.e., pure shear flow), whereas the distal portions may involve significant components of non-coaxial flow (i.e., simple shear flow) [5]. Two-dimensional (2D) strain analysis of deformed mafic enclaves in a dacite flow [9] corroborate these inferences and have further shown that the relative proportion of simple shear increases towards the base of the flow while the contribution of pure shear diminishes at depth. Analogue experiments [11] are consistent with the results of these field-based studies and such models provide additional insight into the relations between finite strain axes (e.g., the strain ellipse) and displace-

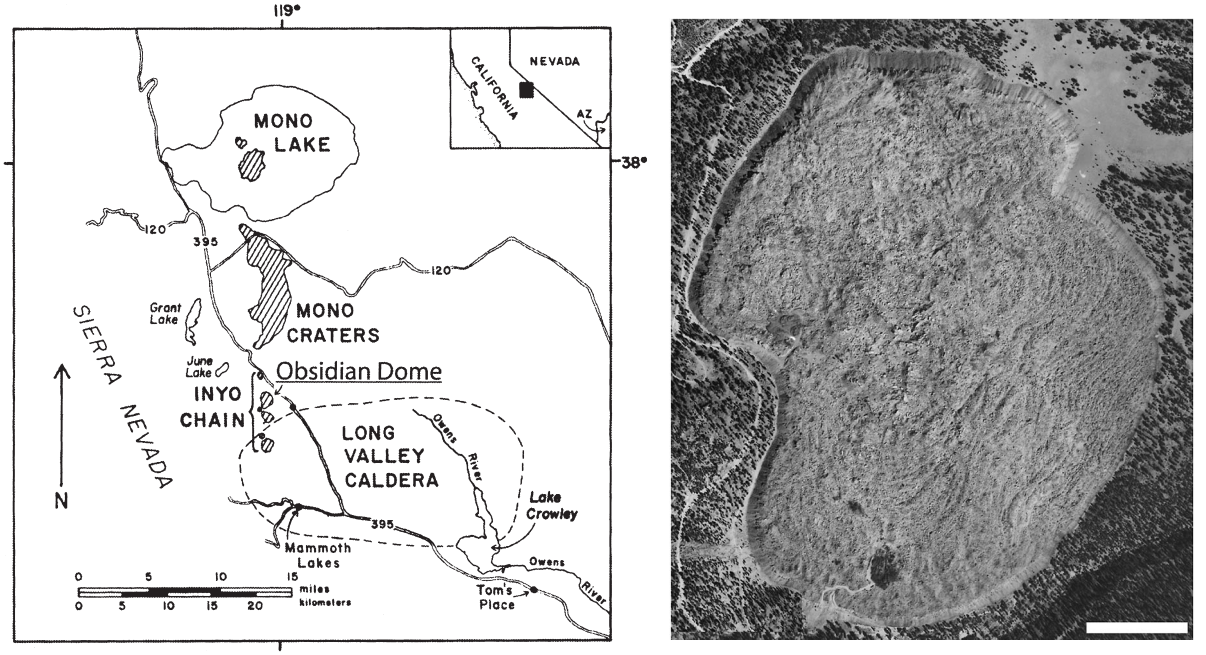

Fig. 1. Location map [23] and aerial photo of Obsidian Dome. North is towards the top of the aerial photo. Scale bar in the aerial photo is about 0.5 km long.

ment directions of lava flows. While the findings of both field-based and experimental studies have shed valuable light on the emplacement mechanisms of silicic lava flows, making it possible to document the dynamics and history of a lava flow through relatively straight forward techniques of modern structural analysis, Ventura [9] notes that "3D strain analyses of lava flows (e.g., basalts and rhyolites) are required to assess the general validity" of mechanical models of lava flow emplacement. The purpose of this paper is to examine 3D orientation distributions of acicular microlites in rhyolitic obsidian (OBS) from Obsidian Dome, CA, USA, as a means of deciphering the emplacement history of this young, well-preserved lava dome (Fig. 1).

Here we use 3D orientation distributions of microlites in OBS to address three fundamental characteristics of flow emplacement: the flow direction, flow regime, and finite strain. First, we show from stereographic analysis that microlite preferred orientation fabrics indicate the local and bulk flow directions along the periphery of the dome. Microlite lineations define a stretching pattern in the lava that we compare to strain patterns produced in analogue experiments [11]. Next, we interpret measured orientation distributions in a theoretical framework in order to elucidate the probable flow type (e.g., pure vs. simple shear). In particular, we show that most of our measured orientation distributions resemble those of dominantly pure shear flow, as predicted by numerical studies [12–14]. We then analyze the variance in microlite trend to estimate the strain acquired during flow. Because "quantitative estimates of the strain accumulated by the magma during flow and data on the partition of deformation are lacking" [9], these strain estimates are useful for determining the relative timing of microlite alignment and the formation of larger-scale flow structures such as surface folds. Strain estimates may also be relevant for understanding how strain is partitioned on scales ranging from microscopic to macroscopic.

Obsidian lavas are well suited for studying flow dynamics because they contain small amounts of microlites, acicular crystals typically less than 10 μm in length (Fig. 2). The characteristically low volume fractions (0.01–0.1) insure that hydrodynamic interactions between microlites are negligible [15,16] and consequently, microlites serve as excellent flow markers. Moreover, their prismatic shape and large aspect ratio make them better flow type and strain indicators than more equant crystals, or those of tabular, cubic, and transitional shapes [14]. Theoretical studies concerning the orientation distribution of rod-shaped crystals in dilute systems provide a framework with which to compare measurements of crystal orientation [17–19]. For example, Manga [13] showed that 3D microlite orientation distributions in OBS from Glass Mountain, CA, USA, when interpreted within a theoretical context, can be used to constrain flow properties such as shear type, strain, and rheology. Obsidian, with its low crystal contents, is therefore a good match for the conditions described in theoretical and computational studies. Techniques developed here may be used to infer strain histories of both older (and more poorly preserved) OBS flows, and samples from volcanic conduits.

2. Background

Obsidian Dome was extruded about 550 yr BP, during the most recent series of rhyolitic eruptions in eastern California [20]. Effusive activity was

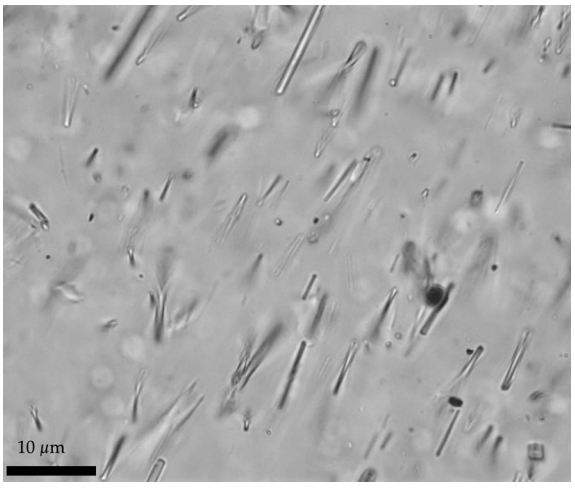

Fig. 2. Photomicrograph of rod-shaped pyroxene microlites in OBS. Scale bar is 10 μm long.

preceded by a series of sub-Plinian eruptions from the Obsidian Dome, Glass Creek, and Deadman vents [20]. This flow is perhaps the most extensively studied OBS flow on Earth, with abundant data on the petrologic and textural development of the flow made available through the Inyo Domes Research Drilling Project [21–25]. Owing to its youth and the arid climate, surface exposures of Obsidian Dome contain a nearly pristine microscopic record of textural and structural evolution.

The lavas that compose Obsidian Dome are texturally and structurally heterogeneous. Fink [10] noted that chemically homogeneous lavas of rhyolitic OBS flows generally exhibit three textural types: coarsely vesicular pumice (CVP), finely vesicular pumice (FVP), and obsidian (OBS). These lavas differ primarily in their vesicularities and microcrystallinities, and boundaries between types may be sharp or gradational. These lavas are all present in varying proportions within Obsidian Dome. CVP has numerous ($>50\%$) large vesicles (diameter >1 mm), while FVP has both lower vesicularity ($<40\%$) and smaller vesicles (diameter <1 mm). Obsidian is, by definition, vesicle poor. The three lava types have consistent contact relations throughout flows and occur in a characteristic stratigraphic order (Fig. 3).

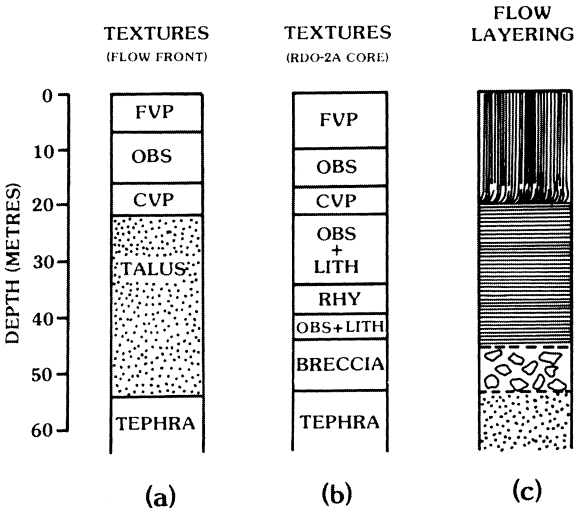

Fig. 3. Textural variations in Obsidian Dome as revealed by (a) flow front exposures and (b, c) research drilling. From [22]. See text for abbreviations.

Microlites are found in the tephra, indicating that they formed prior to the onset of explosive activity (Fig. 2) [25]. Microlites in dome lavas consist of dominantly Ca-poor pyroxene, oxides, and plagioclase feldspar. Flow banding, consisting of alternating microlite-rich and microlite-poor layers, ranging in thickness from about 0.01–1 mm, is ubiquitous in all samples examined. Previous work on the textures and volatile contents of lavas from the flow, conduit, and dike of Obsidian Dome suggests that crystallization began with pre-eruptive growth of phenocrysts and microphenocrysts, followed by pre- to syn-eruptive degassing-induced microlite nucleation and growth, and terminating in static crystallization and devitrification of the slower cooling interior of the dome and vent [25–27].

Work by Miller [20], Fink [28] and the Inyo Domes Research Drilling Project [21] confirmed the presence of a feeder dike beneath the Inyo Domes. Sampson [23] noted that the geometry of surface folds may qualitatively reflect the mean transport direction, and, in the case of Obsidian Dome, reflect the initial eruptive style. Based on the elongate north–south morphology of Obsidian Dome and the geometry of surface folds, Sampson [23] suggested that lava erupted initially from an elongate vent and eventually became localized in a pipe-like conduit during the waning stages of eruption.

3. Methods

OBS samples were collected from 13 locations along the margin of Obsidian Dome (Fig. 4). At the flow front, OBS occurs approximately 10 m below the flow surface, where the lava is exposed in laterally-continuous flow banded outcrops approximately 10–20 m thick. While the base of the OBS layer is obscured by talus, samples were collected from positions that correspond to flow depths of approximately 15 m. All flow front samples were oriented by noting the strike and dip of flow banding, geographic north, and the up-direction on the sample. Samples of near-vent and distal lava were obtained from the Inyo drilling program (courtesy of T. Vogel), which produced

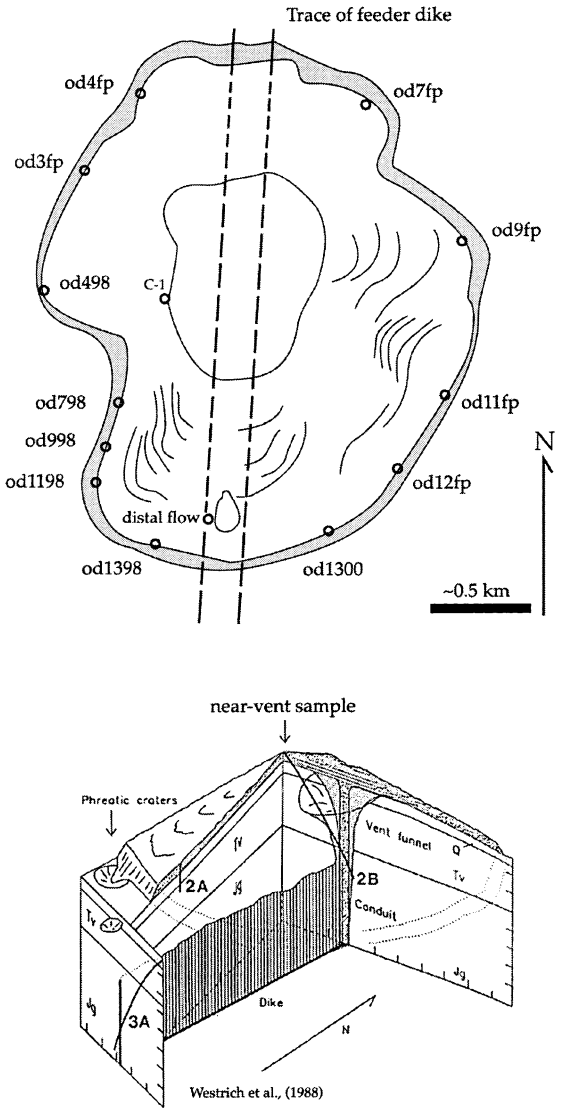

Fig. 4. Map showing locations of samples collected from the periphery, distal flow core RDO-2A, and near-vent (sample C-1; upper map). Lower diagram provides a perspective view of the near-vent (2B) and distal flow core (2A) locations. Modified from [27].

nearly continuous core from the dome, conduit, and dike of the complex (Fig. 4). Conduit core samples (obtained from drill core RDO-2B) are largely microcrystalline, owing to the effects of devitrification. However, one sample collected from a depth of approximately 10 m is glassy and microlites are easily discerned from the matrix glass. This sample is hereafter referred to as the 'near-vent' sample. Although this core sample was not oriented (samples rotated when extracted and core orientations were not well constrained), it contains an important record of relative microstructural development in the near-vent region. In addition, a sample from the distal flow core (RDO-2A) was analyzed from a depth of 47 m. Unlike the other holes, RDO-2A was drilled vertically and consequently, orientations of samples from this core are constrained in terms of their up-directions and orientation with respect to a horizontal plane. This core sample, hereafter referred to as the 'distal flow' sample, comes from a basal OBS layer with prominent horizontal foliations [22]. Thin sections were made in the plane of foliation. Samples from shallower flow depths in core RDO-2A contain a high concentration of angular vesicles, many of which disrupt microlite alignments. Such later-stage textures overprint early flow-induced fabric and thus preclude an accurate analysis of strain history. Hence, we concentrate on the deeper sample in the distal flow core. With the exception of a 12 cm thick glassy margin, the dike is entirely crystalline (drill hole RDO-3A) [29] and consequently microlites are difficult to recognize. We do not include analyses of microlites in the dike because the main focus of this paper is to address the dynamics of subaerial flow.

3.1. Measurement techniques

3D microlite orientation was determined on doubly polished thin sections (30 μm thick) made with the strike of flow bands parallel to the long dimension of the slide and the dip normal to the plane of the slide. Orientation was measured following techniques described in [13] whereby digital reconstructions of microlite size, shape, and orientations are made from a series of high magnification (500×) digital photomicrographs (Fig. 5). Images were collected from successive 2 μm focal planes within a thin section. The outlines and focal points (i.e., the point that is most in focus) of each microlite in each photomicrograph were digitized in a computer-auto-

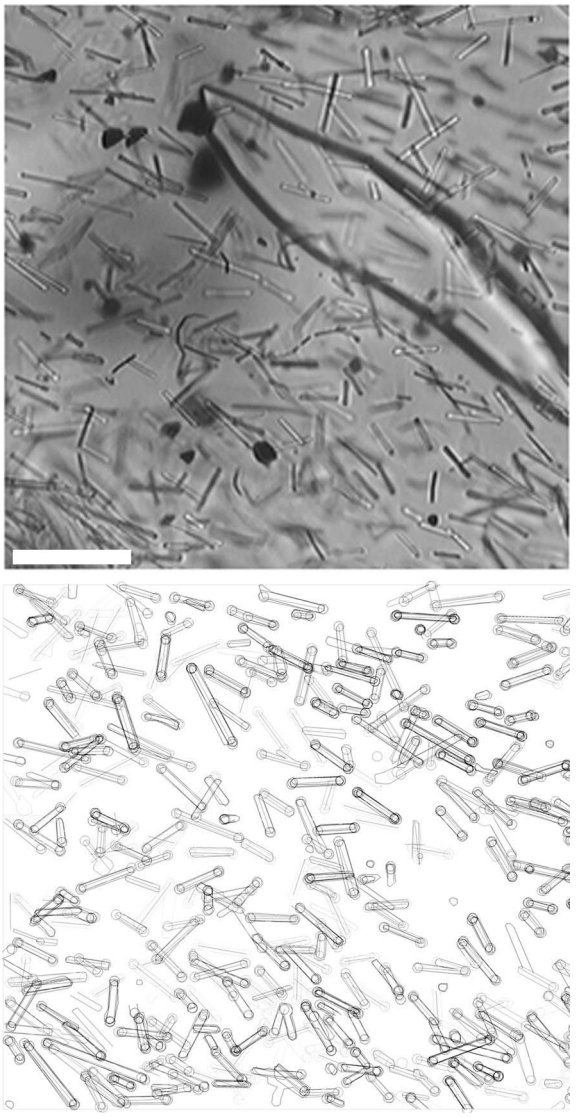

Fig. 5. Photomicrograph of OBS from the near-vent region (top) and a digital reconstruction of this OBS (bottom; sample C-1). Scale bar is approximately 5 μm long and the area in the reconstruction equals that in the photomicrograph. Measurement techniques are described in text and [13].

mated drawing program. Each digitized photomicrograph was shifted relative to the next in the series by 2 μm intervals to produce a stacked array of images which were geometrically consistent with the different focusing planes in the thin section. Next, the series of stacked images was viewed in plan and lines were drawn to connect the focal point markers on each end of the digitized microlite, thus producing a stick representation of the length of each rod-shaped microlite in the thin section (Fig. 5). Microlite length, width, and orientation were calculated from these digital reconstructions.

Due to the tedious nature of digital reconstructions, microlite orientation distributions for nine of the 14 samples were determined from direct measurements on the petrographic microscope. This technique involves measuring apparent microlite length and the difference in vertical position between microlite tips with an optical micrometer built into the petrographic scope and the focusing knob, respectively (Fig. 6). 3D length was calculated using the Pythagorean theorum given the measured values for apparent length and

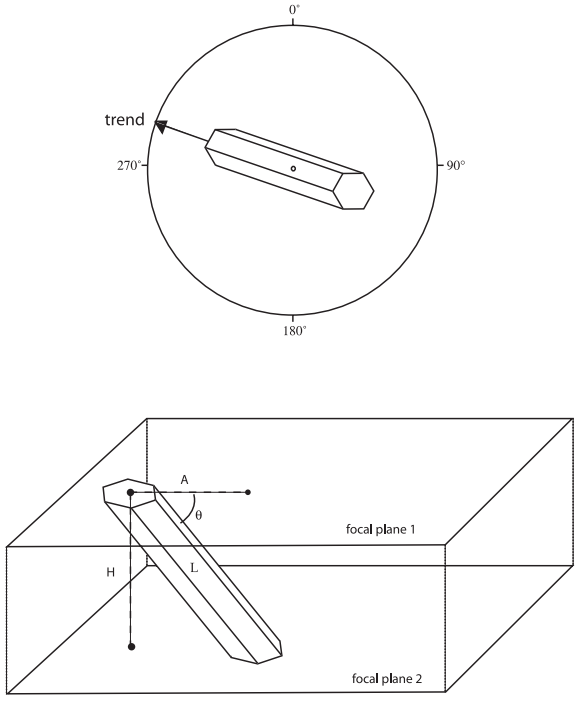

Fig. 6. (Top) Schematic showing how trend angle is determined from comparison of microlite long axis with microscope stage goniometer. (Bottom) 3D length (L) and plunge (θ) are determined from measurements of microlite apparent length (A) and vertical difference in microlite tips (H). Focal planes 1 and 2 are the depths within the thin section where microlite ends are completely in focus.

height difference of each microlite. The plunge of each microlite was calculated trigonometrically once the true length (hypotenuse) and vertical height difference was constrained. Microlite trend was measured with the goiniometer in the microscope stage. These measurements were made at 1000× and carry a precision of about ±0.5 μm.

4. Results

Microlite orientation data are plotted in Fig. 7 together with the measured strike and dip of flow banding at sample locations. Also shown are the axial traces of buckle folds formed in response to cooling and shortening of the uppermost 10 m of the flow [4]. Surface folds appear to be absent on

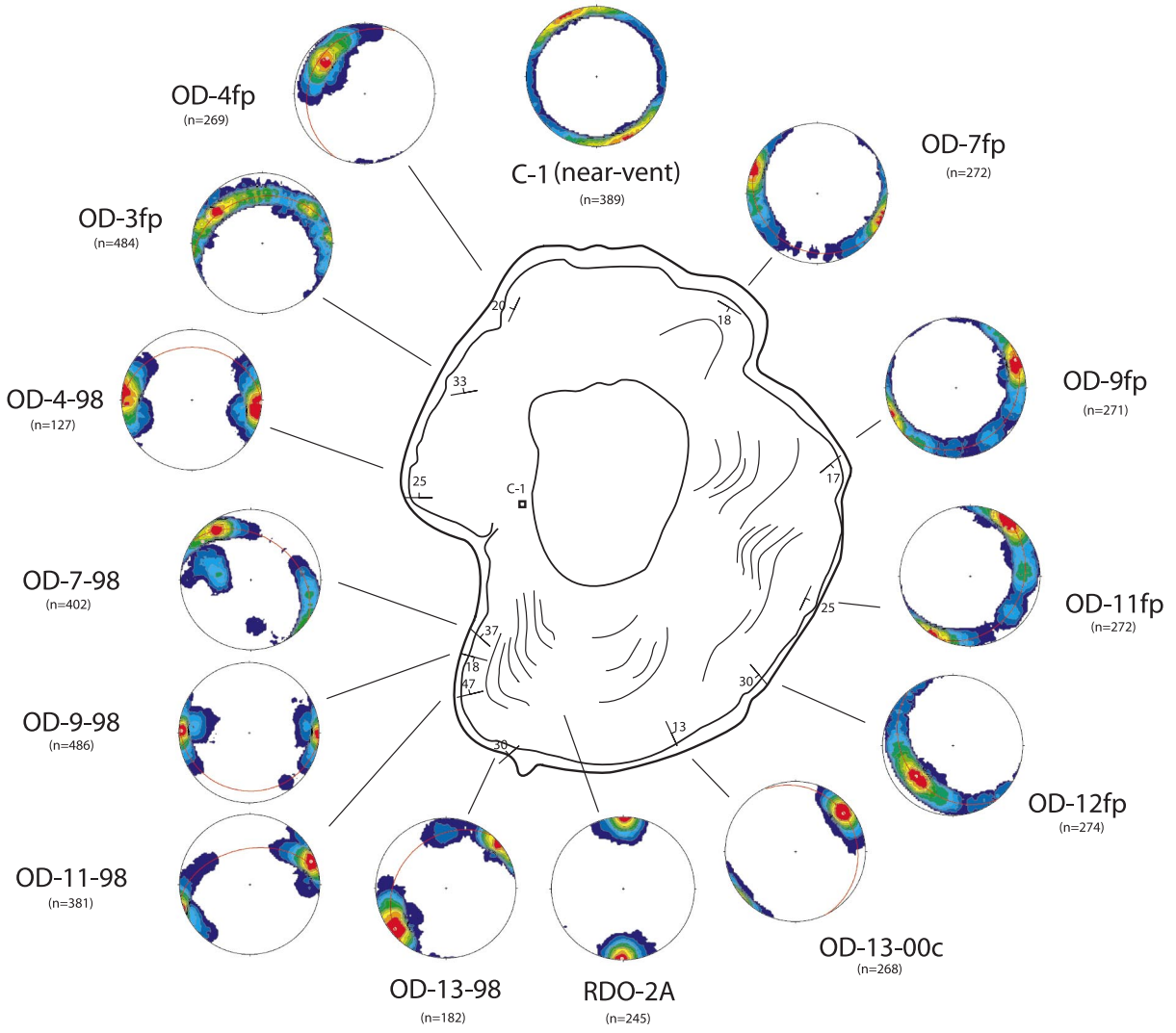

Fig. 7. Microlite orientations in flow front, near-vent (C-1), and distal flow core (RDO-2A) samples. Stereonets show trend and plunge of microlites. The number of microlites measured in each sample is given in parentheses. Red areas signify highly aligned microlites whereas blue demarcates more scattered microlite orientations. Great circles indicate the strike and dip of microlitic flow banding, and the orientation of flow banding. The precise orientation of the near-vent sample is unknown, however, flow banding in the distal flow core sample is horizontal and thus microlite orientations are constrained in terms of their plunge angle and relative degree of alignment, but not their trend.

the northwestern flow lobe. Structural relations along the flow front are indicated by the attitudes of flow banding. Flow banding strikes at high angles to the margin at all but three sample locations and is commonly oriented normal to the flow front. Flow banding in two samples from the northernmost flow margin and one from the eastern margin strike parallel to the flow front. Flow banding dips shallowly ($<30°$) in most samples. As the orientation of surface folds is roughly parallel to the flow front, the orientation of flow banding in most samples is not compatible with the trend of large surface folds.

Microlite trend and plunge data for flow front, distal, and near-vent samples are plotted on lower hemisphere stereographic projections in Fig. 7. The strike and dip of microlite flow banding are plotted as great circles. The data are contoured according to procedures described in [30,31], with only data of statistical significance shown, and variability in orientation frequency depicted as a range of colors. Red corresponds to the highest orientation frequency ($>10\%$) and dark blue the lowest (0–1%). The orientation frequency variation between these colors is linear. Red areas therefore represent microlite populations that are approximately 10 times more aligned than microlites in the dark blue areas. The number of microlites measured, along with size measurements for several flow front samples and the near-vent sample are given in Table 1.

Microlites are well oriented in each of the flow front samples; the red clusters correspond to preferred microlite alignments. Microlites with the highest orientation frequency vary by no more than 15° in trend and 10° in plunge in all samples. Less well-defined secondary lineations appear as yellow and green fields (e.g., in OD-3fp, OD-9fp, and OD-11fp). Microlite lineations do not plunge significantly out of the plane of flow banding, as evidenced by the correspondence of preferred alignments with great circles. Indeed, microlite plunge in most samples does not exceed 30°, and thus, these orientations are compatible with the shallowly dipping character of flow banding. Microstructures are therefore defined by well-developed lineations oriented within the plane of flow banding, similar to 1-s fabrics commonly found in metamorphic tectonites [32]. Most lineations trend parallel to the strike of flow banding. These fabrics are identified by two red clusters on either end of the great circle representing flow banding. In other samples, lineations are inclined to the strike direction. Lineation rake in these samples varies from approximately 10° (e.g., in OD-11-98) to 90° (e.g., in OD-4fp, OD-12fp, and OD-13-00).

When microlite lineation trend is compared to the local geometry of the flow front, two patterns emerge. First, lineations trend at high angles to the flow front along the western margin; this pattern mimics the orientation distribution shown by the strike of flow banding. Trend varies from south–west in the southernmost sample (OD-13-98) to east–west in the western flow (samples OD-4,9,11-98) to north–west in the northern flow (OD-3fp and OD-4fp). While most linear fabrics are horizontal, three lineations plunge shallowly away from the flow front. Second, of the five samples analyzed along the eastern margin of

Table 1
Microlite properties in flow front and near-vent samples measured from digital reconstructions

Sample	No.	Length[a] (μm)	Width (μm)	Aspect ratio	Number density (no./cm^3)	Volume fraction
OD-4-98	127	8.7 (5.1)	2.1	4.2	1.4×10^8	0.020
OD-7-98	402	6.3 (3.4)	1.5	4.1	2.8×10^8	0.014
OD-9-98	486	5.9 (3.7)	1.9	3.1	3.6×10^8	0.028
OD-11-98	381	6.9 (3.6)	1.7	3.9	4.7×10^8	0.032
OD-13-98	182	9.1 (7.2)	1.7	5.4	2.3×10^8	0.028
C-1[b]	389	12.1 (4.8)	2.3	5.4	4.6×10^8	0.090

Length, width, and aspect ratio are mean values.
[a] Values in parentheses are standard deviations of mean length.
[b] Near-vent sample.

the dome, four exhibit flow front parallel lineation attitudes. All of these lineations are flat-lying to shallowly plunging. A single sample (OD-9fp) along the eastern margin shows a flow front normal trend. In summary, we find two preferred microlite orientation fabrics, one in which lineations trend parallel to the flow front and one in which microlites trend approximately normal to the flow front.

Although the sample from the near-vent region was not geographically oriented, orientation data are depicted on a stereonet to show the relative degree of alignment (Fig. 7). In this sample, microlites in the highest orientation density class trend over a range of approximately 25° and plunge less than 10°. The geographic orientation of the distal flow sample is partially constrained in that the drill hole was vertical and thus flow banding attitudes (vertical, diagonal, horizontal) could be determined. The distal flow sample exhibits well-developed horizontal foliations. Microlite orientations are therefore well-constrained in terms of their plunge and relative degree of alignment within the plane of flow banding, but their trend directions relative to geographic north and overall flow geometry are unknown. Microlites in this sample are well aligned and form two semicircular regions on opposite edges of the stereonet (Fig. 7). These orientation clusters demarcate well-developed sub-horizontal lineations lying within the plane of flow banding.

5. Discussion

Measured orientation distributions are the integrated product of bulk and local flow kinematics and reflect the stretching pattern in various parts of the flow. Here we discuss the relations between microlite preferred orientations and the bulk flow direction inferred from the geometry of the flow (i.e., dome shape and flow front orientation). Next, we compare the measured fabrics to stretch trajectories predicted by recent analogue models [11]. These comparisons may provide constraints on the flow regime (e.g., pure and simple shear) operating in different parts of the flow. In the discussion that follows, we show that measured changes in the degree of microlite alignment between a near-vent sample and the flow front provide a means of quantifying the amount of strain (extension) associated with emplacement. These strain values are useful for developing kinematic models [9], understanding larger-scale structures in the flow, and potentially for quantifying strain rates when estimates of emplacement time can be independently assessed. Finally, we discuss applications of these data to analysis of strain features of varying scales and criteria necessary for using microlite fabrics to interpret the emplacement histories of prehistoric flows.

5.1. *Microlite orientation distribution–emplacement mechanism*

Microlite preferred orientations develop during flow in subsurface regions and during flow emplacement. Microlite long axes become aligned in the local extension direction [13], which in the case of a simple shear flow, coincides with the transport direction. In the case of a pure shear flow, the extension direction may be either parallel or normal to the direction of lava transport [11]. At Obsidian Dome, the orientation of large surface fold axes, which develop normal to mean flow direction [10,33], the underlying topography, and the general shape of the dome indicate that the bulk flow direction is normal to the flow front at each location along the margin. The elliptical dome shape suggests that lava spread in a radial fashion away from a roughly elliptical vent [23,34]. The pattern of microlite lineations along the southwestern, western, and northwestern flow margins records this radial flow, as lineations trend at high angles to the flow front and the trend angle varies sympathetically with the orientation of the flow front. Sample OD-9fp, located on the eastern margin, may also record the bulk flow direction at that location, as it too contains a flow front normal lineation.

Along the eastern flow front, margin-parallel preferred alignments suggest that while the bulk flow direction was approximately normal to the flow front, the local extension direction was parallel to the flow front at several locations. These relations suggest that margin-normal shortening

may have played an important role in lineation development along the eastern part of the flow. Compression of the flow against a topographic barrier or talus apron may have influenced the local extension direction and thus could have caused earlier-formed lineations with margin-normal alignments to rotate to their present margin-parallel positions. Indeed, surface folds are well developed on the eastern flow lobe where topography is slightly elevated immediately outboard of the flow periphery; such folds are poorly developed, if not absent on the western portions of the flow. Fink [10] documents a similar, although larger-scale deformation pattern on the northwest and northeastern lobes of Little Glass Mountain, CA, where overturned margin-parallel folds developed during flow advance. The shortening that accompanies fold formation would be accommodated by stretching parallel to the hinge lines of these folds, and consequently, microlites would align parallel to fold hinge lines.

Preferred mineral alignments and stretched bubble fabrics have often been cited to indicate transport directions [2,35,36]. Our results indicate that the stretching direction in a 3D flow may sometimes be perpendicular to the flow direction.

Further insight into the origin of lineations and the emplacement mechanism of Obsidian Dome comes from comparing microlite lineation patterns to strain patterns produced in experimental studies using analogue fluids. Merle [11] showed that viscous silicone putty spreading radially at the end of a channel over a solid horizontal base experiences two shear regimes: (1) dominantly simple shear at the base and (2) dominantly pure shear at the surface. The local proportions of pure and simple shear also vary as a function of spreading time, or lateral position within the flow, with the near-vent flow dominated by pure shear where gravity collapse drives motion, and distal flow experiencing increasing amounts of simple shear. Field-based measurements of mesoscopic and macroscopic structures [5,9] confirm these experimental findings. Merle [11] further demonstrates that pure and simple shear regimes correspond to a concentric stretch trajectory (extension normal to flow) and a radial stretch trajectory (extension parallel to flow), respectively. Concentric stretching is accompanied by radial horizontal shortening and a component of vertical shortening due to spreading. Thus, the pure shear regime is a 3D deformation. Concentric stretching creates shallow flow-normal stretching fabrics and surface folds, while radial stretching produces preferred mineral alignments and stretched bubbles parallel to the flow direction. These stretching regimes are separated by a narrow zone of zero preferred stretching [11]. Similar strain patterns have been produced in other experimental studies [37].

Stretching patterns documented by Merle [11] are governed by the local proportions of simple and pure shear and are thus indicative of a flow's emplacement mechanism. We see evidence of both radial and concentric stretching patterns in microlite orientation distributions along the Obsidian Dome margin. Fabrics exposed along the western flow front reflect radial stretching, possibly due to simple shear kinematics, while most samples along the eastern margin may have developed in accordance with concentric stretching in a dominantly pure shear flow. The presence of both types of stretching fabrics at approximately the same level ($\sim$15 m) within the flow may reflect the proximity of these samples to the sharp transition from concentric to radial stretching computed by Merle [11]. According to Merle's [11] computations, the change from concentric stretching (top) to radial stretching (base) is instantaneous, without an intermediate stretch orientation. Two samples exhibiting oblique lineations along the flow front (OD-7-98, OD-13-98) are inconsistent with these results [11]. The oblique lineations may be due to local strain perturbations caused by irregularities in topography or flow rheology. Sample OD-13-98 is indeed positioned on the edge of a phreatic pit where the southern flow lobe partially fills and obscures this depression. Both samples (OD-7-98, OD-13-98) have weakly developed secondary lineations that trend approximately normal to the flow front (Fig. 7). We interpret the secondary microstructures in these samples to record part of an integrated strain path consisting of both early and later flow-induced fabrics.

In summary, the measured stretching patterns

show that, on the scale of the entire flow, a heterogeneous deformation field develops in the uppermost OBS layer. Interaction of the flow with topography is probably important in modifying early formed fabrics. Comparison of fabrics developed in natural lavas to those produced in relatively simple analogue systems provides a useful means of interpreting the flow emplacement mechanism. Such comparisons may be especially helpful when surface structures such as folds are poorly developed or difficult to recognize due to brecciation of the flow carapace.

5.2. Strain history

Comparison of the variance in microlite orientation distributions of near-vent, distal, and flow front samples provides an estimate of the strain acquired during flow emplacement. We expect scatter in orientation distributions to decrease with increasing deformation as "the degree of preferred orientation along the direction of elongation in the deforming material increases" [18]. Glassy lavas are particularly well-suited for studying lava flow dynamics because microlite concentration is within the dilute limit (volume fractions $c \ll 1$; Table 1) and hydrodynamic interactions among crystals are negligible [13,15,16]. Despite the low abundance of microlites in these lavas, many of the samples contain abundant microphenocrysts and phenocrysts, which disrupt microlite orientations. Indeed, much of the scatter in orientation is due to local dispersion of microlite long axes around larger objects. To isolate the effects of flow on microlite orientation distributions, we have selected for analysis a flow front sample (OD-13-00) that contains relatively minor amounts of microphenocrysts and phenocrysts. In this sample, microlite orientation fabrics are undisturbed by flowage around bubbles, phenocrysts, and microphenocrysts. We also include analysis of the distal flow sample, as it too appears devoid of microphenocrysts and bubbles and thus provides important strain information from the flow base.

A theoretical framework exists for describing the behavior of rod-shaped particles in pure and simple shear flows [17,18]. The theoretical results apply to systems that: (1) are sufficiently dilute that mineral grains are widely spaced, (2) exhibit plane strain deformation resulting from flow, and (3) have Newtonian flow rheologies. Blanchard et al. [12] and Manga [13] used these formulations to compute the resultant orientation distributions of crystal-bearing magmas flowing, respectively, in a dike and on the surface. These studies show that acicular crystals in a low Reynolds number flow will develop distinct orientation distributions depending on the type of shear involved (e.g., pure vs. simple shear flows) and the amount of shearing [14]. Manga [13] characterizes the orientation distribution of microlites in Medicine Lake (CA) OBS in terms of standard deviations of microlite trend (σ_ϕ) and plunge (σ_θ). He shows that while both of these values approach zero with increasing strain in a pure shear flow (i.e., crystals become aligned in the flow plane and with the direction of extension), they approach finite constants in a simple shear flow owing to periodic particle rotations. Most notable are the differences in (σ_θ) between pure and simple shear flows. Specifically, in a simple shear flow, σ_θ reaches a minimum value of $\sim 20°$ for rod-shaped crystals of aspect ratio 10 and strains greater than 10. In contrast, σ_θ is zero at an equivalent strain in a pure shear flow. Distinct orientation distributions are therefore attributable to the type of shearing and the amount of strain.

The models described above apply to flows undergoing plane strain. In a natural flow, the pure shear component may correspond to a 3D deformation, as was demonstrated by [11]. Strain estimates derived from comparing measured orientation distributions in OBS to those predicted by theory will therefore only yield approximate values. The studies nonetheless provide an important framework for inferring accumulated strain from orientation measurements, as models describing orientation distributions resultant from 3D flows are lacking. Fig. 8 shows histograms of microlite trend (ϕ) and plunge (θ) (inset) for the near-vent, distal, and flow front samples, from which σ_ϕ and σ_θ are calculated. These distributions show that (1) microlites are better aligned in the flow front and distal flow than in the near-vent region, and (2) very good microlite

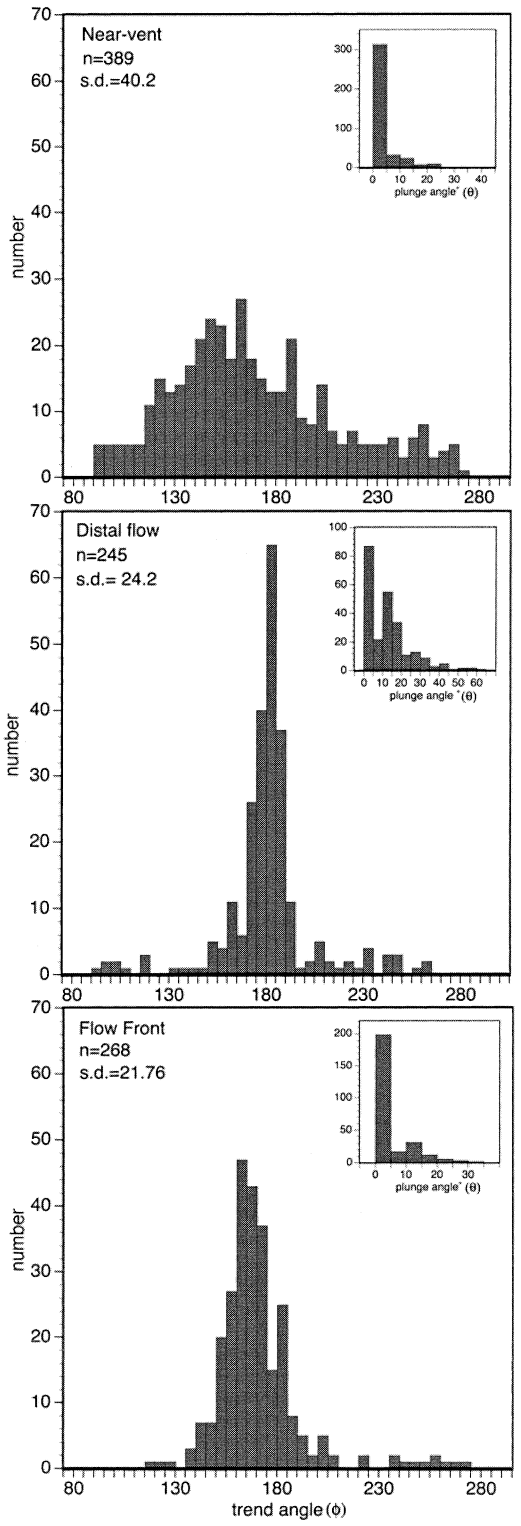

Fig. 8. Histograms of microlite trend and plunge (insets) for the near-vent sample (top), distal flow (middle), and a flow front sample OD-13-00 (bottom). Trend and plunge are measured in degrees. The total number of microlites measured in each sample (n) is given in addition to the standard deviation of microlite trend (s.d.). Microlites are better aligned in the flow front as indicated by the narrower trend distribution. Microlites are well aligned within the plane of flow banding in all samples, however, the relatively broader (θ) distribution in the distal flow may reflect the influence of basal shear stress (see text).
←

alignment within the plane of flow banding is developed in all samples, as evidenced by their narrow (θ) distributions. Analysis of variance indicates that σ_ϕ decreases by about a factor of two between the vent (40.2°) and flow front (21.8°), with an intermediate value (24.2°) in the distal flow sample. σ_θ shows little variation in the near-vent and flow front regions and is small ($\sim$6.5°) in both of these samples. Small σ_θ values suggest dominantly pure shear kinematics in the near-vent and flow front [13]. In contrast, σ_θ is about twice as large (12.7°) in the distal flow sam-

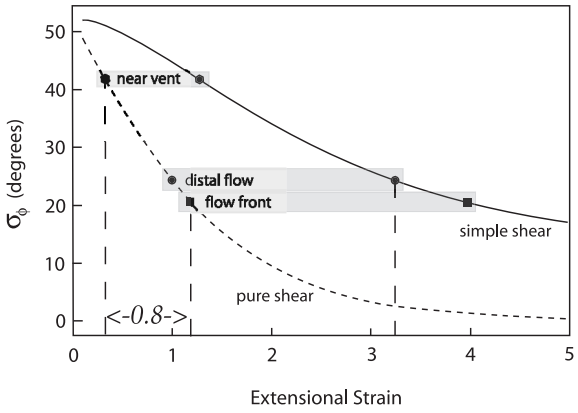

Fig. 9. Numerically derived curves showing the standard deviation of microlite trend (σ_ϕ) versus extensional strain for rod-shaped microlites of aspect ratio 5 in simple (solid) and pure shear flows (dashed). Intersections of curves with extrapolated standard deviations for a near-vent sample (hexagons), distal flow sample (circles), and flow front sample OD-13-00 (squares) yield estimates of strain due to flow across the surface. The difference in pure shear strain between the flow front and near-vent region ($\sim$0.8) is an estimate of the strain associated with flow emplacement.

ple. We interpret the higher σ_θ in this sample to reflect the influence of basal shear stress and an inherited component of simple shear strain [13] due to its location near the flow base.

Fig. 9 shows numerically determined curves of σ_ϕ versus extensional strain for microlites of aspect ratio 5 in dilute pure and simple shear flows. The calculations assume plane strain, an initially random orientation distribution, and that the suspension consists of non-interacting microlites (i.e., $c \ll 1$; valid for dilute suspensions). Given the strong component of pure shear strain indicated by map patterns (e.g., Section 5.1) and small σ_θ, we plot σ_ϕ for near-vent and flow front samples on the pure shear curve to estimate strain. Values for the distal flow sample are also shown for comparison. Graphical relations indicate strains of approximately 0.3 and 1.1 for near-vent and flow front samples, respectively. By virtue of their position, microlites in the flow front traveled farther than microlites in the near-vent region, and thus accumulated more strain than the near-vent sample. Some of the difference in strain values may also reflect the effects of vesiculation near the vent and bubble collapse in the flow [34,38]. Indeed, the near-vent sample contains a few bubbles (volume fraction of a few percent); assessing the amount of bubble collapse in the flow is difficult and controversial [34,39]. Disruption of previously developed, vent-inherited microlite alignments by bubble growth and deformation effectively resets the orientation distribution in the vent and thus, the difference in strain values (0.8) provides an estimate of extensional strain associated with flow emplacement.

It is likely that flow in Obsidian Dome had components of both pure and simple shear, and consequently the estimates of pure shear strain inferred from orientation distributions serve as a lower bound for the possible strain experienced during emplacement. For example, if flow in the distal portions of Obsidian Dome were characterized by simple shear, a strain of about 3.2 (the value for the distal flow sample on the simple shear curve, Fig. 9) may be a meaningful estimate of the strain experienced during flow on the surface. This assumes that microlites at an equivalent depth (47 m) in the near-vent region are randomly oriented. We are cautious about this estimate because we have no constraints on microstructures within deep parts of the vent. Nonetheless, our pure shear strain estimate is of similar magnitude as the range (1–1.6) determined by Ventura [9] for a dacitic lava flow of similar dimensions (radius $\sim$1 km). Pure and simple shear strain estimates in near-vent, distal, and flow front samples bracket the strain accrued during emplacement.

Strain estimates are useful for determining the relative timing of microlite alignment and the formation of larger-scale structures in OBS flows. The approximate timing of preferred microlite orientation can be assessed by comparing strain inferred from orientation distributions (e.g., Fig. 9) with the total strain experienced during flow on the surface. We consider the emplacement of the dome as a homogeneous fluid spreading radially under the influence of gravity. We assume flow front samples experienced a large component of pure shear strain as a result of lateral spreading of the flow. The strain due to axial spreading of the flow can be estimated using an average dome radius of 750 m and a mean thickness of 50 m [34]. Flow volume (assumed constant) based on these dimensions is approximately 0.1 km^3. The equivalent radius of a sphere of equal volume is 290 m. Horizontal spreading of this fluid sphere yields an extensional strain (i.e., pure shear) of about 1.6. This pure shear estimate is similar to the strain of $\sim$1 inferred from Fig. 9, and therefore suggests that flow on the surface was sufficient to produce the preferred alignments in the flow front. Extensional strain inferred from orientation distributions is also similar in magnitude to shortening strains recorded in mesoscopic folds (usually < 1) and large surface folds that develop during flow advance. This similarity suggests that extensional and shortening strains are compatible across a range of scales and that the contrasting styles of deformation (i.e., extension vs. shortening) may have occurred contemporaneously.

Strain determined from orientation measurements may also provide a check on estimates of eruption duration and flow rate derived from analyses of flow morphology [40]. Fink and Griffiths [40] used observations of overall flow morphology and results from laboratory experiments

to infer emplacement rates and durations for a series of prehistoric rhyolite and dacite flows, including Obsidian Dome. Their simulations suggest emplacement times of about 400 days and corresponding flow rates of 0.6–11 m^3/s for the Obsidian Dome eruption. A strain of 0.8 inferred from microlite orientations accrued over 400 days implies a strain rate of about 2.3×10^{-8} s^{-1}. The average volumetric flow rate of 5 m^3/s inferred from dome morphology [40] divided by the total dome volume [40] yields an approximate strain rate of 3×10^{-8} s^{-1}. The consistency of these strain rates suggests that estimates of flow rate [40] for the Obsidian Dome eruption are good, as larger strains recorded in the dome would imply larger strain rates for a corresponding emplacement time of 400 days.

Our strain estimates can also be used to assess emplacement times of OBS eruptions if independent estimates of strain rates are available. Currently there are no direct estimates of strain rate for OBS eruptions, however, promising new microstructural techniques are being developed to determine shear rate and flow type in OBS lavas [41].

6. Conclusions

3D microlite orientation distributions measured in OBS are used to place constraints on the emplacement conditions and strain history of Obsidian Dome, CA. These measurements reveal the microscopic strain pattern (i.e., stretching directions) in the shallow parts of the flow periphery, and provide a basis for estimating strain associated with flow emplacement. The results of this study should be applicable to analyses of other glassy lava domes provided they contain dilute quantities of acicular microlites. The salient findings of this study are summarized below.

1. Microlite lineations are well developed in all samples. In many samples, lineations reflect local stretching directions, which may differ from broad-scale flow patterns. Thus, paleoflow directions based on orientation distributions of a few samples may be misleading, and we suggest that several samples be analyzed along a flow periphery to resolve the bulk flow direction. Additionally, microstructures should be analyzed in the context of large-scale flow structures (e.g., surface folds) to elucidate flow emplacement dynamics and kinematics.
2. Our measurements of small σ_θ, in both near-vent and flow front samples suggest that flow surface (upper 15 m) samples record predominantly pure shear flow during emplacement. This finding is consistent with results from analog models [11], field-based studies [5,9], and numerical simulations [14] and suggests that flow emplacement was gravity-driven and can be modeled as simple viscous spreading [9,11]. Analysis of a distal flow sample from near the base suggests that simple shear may be more important at depth.
3. Strains of approximately 1 are inferred from the orientation distributions of a near-vent and flow front sample. This estimate reflects part of the bulk strain acquired during transport of lava from the vent to the flow margin, and thus is a measure of strain associated with emplacement. This value coincides with strain measured in mesoscopic and large-scale surface folds [5,6]. It also matches the value for coaxial spreading of a viscous blob of equal volume and thus suggests that flow on the surface is sufficient to produce microlite alignments. Microlite preferred orientations may therefore yield valuable insights into paleoflow directions and paleoslope attitude of ancient and highly dissected lava flows.
4. Estimates of flow emplacement time can be calculated from strain and independent estimates of strain rate. To date, there are no published values for strain rates in OBS flows. This highlights the need for continued study into the kinematics and microstructural character of glassy lavas.

Acknowledgements

This work was supported by NSF Grant EAR-9805305. Thomas Vogel generously provided thin sections of core samples. Helpful reviews from

Oliver Merle and an anonymous reviewer greatly improved this manuscript. *[SK]*

References

[1] E. Canon-Tapia, G.P.L. Walker, E. Herrero-Bervera, The internal structures of lava flows-insights from AMS measurements I: Near vent a′a, J. Volcanol. Geotherm. Res. 70 (1996) 21–36.

[2] D. Shelley, Determining paleo-flow directions from groundmass fabrics in the Lyttelton radial dykes, New Zealand, J. Volcanol. Geotherm. Res. 25 (1985) 69–79.

[3] G. Ventura, R. DeRosa, E. Colletta, R. Mazzuoli, Deformation patterns in high viscosity lava flow inferred from crystal preferred orientation and imbrication structures: an example from Salina (Aeolian Island, S. Tyrrhenian Sea, Italy), Bull. Volcanol. 57 (1996) 555–562.

[4] J.H. Fink, Surface folding and viscosity of rhyolite flows, Geology 8 (1980) 250–254.

[5] J.V. Smith, H.C. Houston, Folds produced by gravity spreading of a banded rhyolite flow, J. Volcanol. Geotherm. Res. 63 (1994) 89–94.

[6] J. Castro, K.V. Cashman, Constraints on rheology of obsidian lavas based on mesoscopic folds, J. Struct. Geol. 21 (1999) 807–819.

[7] Q. Williams, O.T. Tobish, Microgranitic enclave shapes and magmatic strain histories: constraints from drop deformation theory, J. Geophys. Res. 99 (1994) 24359–24368.

[8] R. DeRosa, R. Mazzuoli, G. Ventura, Relationships between deformation and mixing processes in lava flows: a case study from Salina (Aeolian Islands, Tyrrhenian Sea), Bull. Volcanol. 58 (1996) 286–297.

[9] G. Ventura, The strain path and emplacement mechanism of lava flows: an example from Salina (southern Tyrrhenian Sea, Italy), Earth Planet. Sci. Lett. 188 (2001) 229–240.

[10] J.H. Fink, Structure and emplacement of a rhyolitic obsidian flow: Little Glass Mountain, Medicine Lake Highland, northern California, Geol. Soc. Am. Bull. 94 (1983) 362–380.

[11] O. Merle, Internal strain within lava flows from analogue modelling, J. Volcanol. Geotherm. Res. 81 (1998) 189–206.

[12] J.P.L. Blanchard, P. Boyer, C. Gagny, Un nouveau critere de sens de mise en place dans une caisse filonienne le 'pincement' des mineraux aux epontes, Tectonophysics 53 (1979) 1–25.

[13] M. Manga, Orientation distribution of microlites in obsidian, J. Volcanol. Geotherm. Res. 86 (1998) 107–115.

[14] G. Iezzi, G. Ventura, Crystal fabric evolution in lava flows: results from numerical simulations, Earth Planet Sci. Lett. (in press).

[15] M. Rahnama, D.L. Koch, E.S.G. Shaqfeh, The effect of hydrodynamic interactions on the orientation distribution in a fiber suspension subject to simple shear flow, Phys. Fluid. 7 (1995) 487–506.

[16] C.A. Stover, D.L. Koch, C. Cohen, Observations of fibre orientation in simple shear flow of semi-dilute suspensions, J. Fluid. Mech. 238 (1992) 277–296.

[17] G.B. Jeffrey, The motion of ellipsoidal particles immersed in a viscous fluid, Proc. R. Soc. Lond. A 102 (1922) 161–179.

[18] N.C. Gay, Orientation of mineral lineation along the flow direction in rocks a discussion, Tectonophysics 3 (1966) 559–562.

[19] L.G. Leal, The slow motion of slender rod-like particles in a second-order fluid, J. Fluid. Mech. 69 (1975) 161–179.

[20] C.D. Miller, Holocene eruptions at the Inyo volcanic chain, California: Implications for possible eruptions in Long Valley Caldera, Geology 13 (1985) 14–17.

[21] J.C. Eichelberger, C.D. Miller, L.W. Younker, 1984 drilling results at Inyo Domes, California, EOS Trans. AGU 66 (1985) 384.

[22] J.H. Fink, C.R. Manley, Origin of pumiceous and glassy textures in rhyolite flows and domes, in: J.H. Fink (Ed.), The Emplacement of Silicic Domes and Lava Flows, Geol. Soc. Am. Spec. Pap. 212 (1987) pp. 77–89.

[23] D.E. Sampson, Textural heterogeneities and vent area structures in the 600-year-old lavas of the Inyo volcanic chain, eastern California, Geol. Soc. Am. Spec. Pap. 212 (1987) 89–101.

[24] T.A. Vogel, L.W. Younker, B.C. Schuraytz, Constraints on magma ascent, emplacement and eruption: Geochemical and mineralogical data from drill-core samples at Obsidian Dome, Inyo Chain, California, Geology 15 (1987) 405–408.

[25] S.E. Swanson, M.T. Naney, H.R. Westrich, J.C. Eichelberger, Crystallization history of Obsidian Dome, Inyo Domes, California, Bull. Volcanol. 51 (1989) 161–176.

[26] B.E. Taylor, Degassing of Obsidian Dome rhyolite, Inyo volcanic chain, California, in: H.P. Taylor, Jr., J.R. O'Neil, J.R. Kaplan (Eds.), Stable Isotope Geochemistry: A Tribute to Samuel Epstein, Geochem. Soc. (1991) pp. 339–353.

[27] H.R. Westrich, H.W. Stockman, J.C. Eichelberger, Degassing of rhyolitic magma during ascent and emplacement, J. Geophys. Res. 93 (1988) 6503–6511.

[28] J.H. Fink, The geometry of silicic dikes beneath the Inyo Domes, California, J. Geophys. Res. 90 (1985) 1127–1133.

[29] T.A. Vogel, J.C. Eichelberger, L.W. Younker, B.C. Schuraytz, J.P. Horkowitz, H.W. Stockman, H.R. Westrich, Petrology and emplacement dynamics of intrusive and extrusive rhyolites of Obsidian Dome, Inyo Craters Volcanic Chain, eastern California, J. Geophys. Res. 94 (1989) 17937–17956.

[30] W.B. Kamb, Ice petrofabric observations from Blue Glacier, Washington, in relation to theory and experiment, J. Geophys. Res. 64 (1959) 1891–1909.

[31] W.B. Kamb, Theory of preferred orientation developed by crystallization under stress, J. Geol. 67 (1959) 153–170.

[32] G. Davis, Structural Geology of Rocks and Regions, John Wiley and Sons, New York (1984) 492 pp.
[33] J.H. Fink, R.C. Fletcher, Ropy pahoehoe: Surface folding of a viscous fluid, J. Volcanol. Geotherm. Res. 4 (1978) 151–170.
[34] J.C. Eichelberger, C.R. Carrigan, H.R. Westrich, R.H. Price, Non-explosive silicic volcanism, Nature 323 (1986) 589–602.
[35] M.P. Coward, The analysis of flow profiles in a basaltic dike using strained vesicles, J. Geol. Soc. Lond. 137 (1980) 605–615.
[36] M. Polacci, P. Papale, The evolution of lava flows from ephemeral vents at Mount Etna: insights from vesicle distribution and morphological studies, J. Volcanol. Geotherm. Res. 76 (1997) 1–17.
[37] S. Blake, Viscoplastic models of lava domes, in: J.H. Fink (Ed.), Lava flows and Domes: Emplacement Mechanisms and Hazard Implications, IAVCEI Proc. Volcanol. 2 (1990) pp. 208–243.
[38] M.V. Stasiuk, J. Barclay, M.R. Carroll, C. Jaupart, J.C. Ratte, R.S.J. Sparks, S.R. Tait, Degassing during magma ascent in the Mule Creek vent (USA), Bull. Volcanol. 58 (1996) 117–130.
[39] J.H. Fink, S.W. Anderson, C.R. Manley, Textural constraints on effusive silicic volcanism: Beyond the permeable foam model, J. Geophys. Res. 97 (1992) 9073–9083.
[40] J.H. Fink, R.W. Griffiths, Morphology, eruption rates, and rheology of lava domes: Insights from laboratory models, J. Geophys. Res. 103 (1998) 527–545.
[41] A.C. Rust, M. Manga, K.V. Cashman, Determining flow type and shear rate in magmas from bubble shapes and orientations, EOS Trans. AGU 82 (2001) 47.